Int. Symp. on Dynamics and Statistics of Coherent Structures in Turbulence, Oct. 2002, Tokyo, pp. 65-74

Reynolds Number Effect on Feedback Control of Wall Turbulence

Kaoru Iwamoto, Nobuhide Kasagi & Yuji Suzuki

Department of Mechanical Engineering, The University of Tokyo, Hongo, Bunkyo-ku, Tokyo, 113-8656 Japan

Direct numerical simulation of turbulent channel flow at $Re_\tau = 110 \sim 650$ is made in order to assess the feedback control algorithms which have been proposed for reducing skin friction. The effectiveness of the existing control schemes is decreased with increasing the Reynolds number from $Re_\tau = 110$ to 300. It is found, through the Karhunen-Loève (KL) decomposition of turbulent fluctuations, that the KL modes around $y^+ = 20$, which correspond to the longitudinal vortices and near-wall streaky structures, play a dominant role in the production of turbulent kinetic energy and wall shear stress at $Re_\tau = 110$. The nonlinear interaction acts as sink for the turbulence energy of vortical structures at $y^+ \sim 20$, and the energy is transferred toward/away from $y^+ \sim 20$. On the other hand, when the Reynolds number increases, vortical structures at $y^+ \sim 20$ gains energy through the nonlinear interaction from the structures at $20 < y^+ < 100$. It is also found that direct interaction between inner ($y^+ < 100$) and outer ($y^+ > 100$) layers has minor effect on near-wall dynamics even at $Re_\tau = 650$.

1 Introduction

In the last few decades, transport mechanism of wall turbulence has been examined in detail. It is found through direct numerical simulation (DNS) of low-Reynolds-number wall turbulence that near-wall streamwise vortices play a dominant role in the turbulence energy production, wall shear stress and wall heat flux [1, 2]. However, characteristics of coherent structures at higher Reynolds numbers still remain unresolved, since various Reynolds number effect on wall turbulence is observed [3, 4].

From a viewpoint of saving energy and protecting the environment, it is needed to develop efficient turbulence control techniques for drag reduction and/or heat transfer augmentation. Among various methodologies, active feedback control scheme attracts much attention because of its large control effect with small power input [5, 6]. Choi et al.[7] employed local blowing/suction on the wall, which is exerted to oppose the wall-normal velocity fluctuation in the buffer layer (V-control), and obtained approximately 25% drag reduction in their DNS of turbulent channel flow. Bewley et al.[8] showed that the turbulent channel flow could be ultimately

relaminarized by an optimal control scheme. Although these control schemes have demonstrated marked effectiveness, it is not straight forward to employ them in real applications, because they inevitably require sensing at numerous points inside the flow field. Recently, control algorithms using only wall variables have been developed. Lee et al.[9] proposed a suboptimal control algorithm based on the linearized Navier-Stokes equation, and obtained a simple analytical formula determining the control input based on the wall variables. These pioneering studies have demonstrated that the active feedback control of wall turbulence is promising and can be implemented in a real system with the aid of the emergent fabrication technologies such as MEMS.

However, the Reynolds numbers assumed in most previous studies are about $Re_\tau \sim 100$, which is defined based on the wall friction velocity u_τ, the channel half-width δ and kinematic viscosity ν, where significant low-Reynolds-number effects must exist. Therefore, assessment of the existing control schemes at higher Reynolds numbers should be undertaken.

The final goal of the present work is to develop a control algorithm applicable to high Reynolds number flows. Iwamoto et al.[10] have shown the Reynolds number effect on wall turbulence through the Karhunen-Loève (KL) decomposition at $Re_\tau = 110$ and 300. In the present study, the contribution of coherent structures to the wall shear stress and nonlinear interaction between vortical structures are examined through the KL decomposition up to $Re_\tau = 650$ with finer resolution for the inner layer structures.

2 Numerical Method and Control Algorithm

The numerical method used in the present study is almost the same as that of Kim et al.[11]; a pseudo-spectral method with Fourier series is employed in the streamwise (x) and spanwise (z) directions, while a Chebyshev polynomial expansion is used in the wall-normal (y) direction. A fourth-order Runge-Kutta scheme and a second-order Crank-Nicolson scheme are used for time discretization of the nonlinear terms and the viscous terms, respectively. The computational conditions are summarized in Table 1. The Reynolds number Re_τ is chosen as 110, 150, 300, 400, and 650. The flow rate is kept constant at each Reynolds number. Although it is not shown here, turbulence statistics of the present computation for plane channel flow are in good agreement with the DNS data of Moser et al.[3], and are available on the web page at http://www.thtlab.t.u-tokyo.ac.jp. Hereafter, u, v, and w denote the velocity components in the x-, y-, and z-directions, respectively. Superscript ($^+$) represents quantities non-dimensionalized with u_τ and ν.

In order to evaluate the efficiency of feedback control algorithms at various Reynolds numbers, V-control scheme [7] and the suboptimal control [9] are adopted. In both cases, the control input is local blowing/suction at the wall. In the V-control, it is given as:

$$v^+_{wall} = -\alpha\, v^+\Big|_{y^+=10} \tag{1}$$

For the suboptimal control scheme, square of the wall-normal gradient of the spanwise velocity is included in the cost function, and this leads to the control input:

$$\hat{v}^+_{wall} = \alpha \frac{ik_z}{k} \left.\frac{\partial \hat{w}^+}{\partial y^+}\right|_{wall}, k = \left(k_x^2 + k_z^2\right)^{1/2} \tag{2}$$

where ($\hat{}$) denotes the Fourier coefficient. In Eq. (2), k_x and k_z denote wavenumbers in the x- and z-directions, respectively. The positive constant α is chosen in such a way that the power

Table 1: Basic conditions of DNS of turbulent channel flow (Δy_c^+ is the y-interval at the channel center).

Re_τ	Computational periods		Grid points	Grid spacings		
	L_x	L_z	N_x, N_y, N_z	Δx^+	Δy_c^+	Δz^+
110	$5\pi\delta$	$2\pi\delta$	96, 65, 96	18.0	5.40	7.20
150	$5\pi\delta$	$2\pi\delta$	128, 97, 128	18.4	4.91	7.36
300	$2.5\pi\delta$	$\pi\delta$	128, 193, 128	18.4	4.91	7.36
400	$2.5\pi\delta$	$\pi\delta$	192, 257, 192	16.4	4.91	6.54
650	$2.5\pi\delta$	$\pi\delta$	288, 257, 384	17.7	7.98	5.32

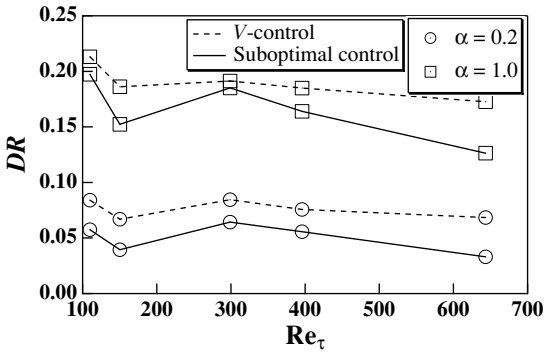

Figure 1: Dependence of drag reduction rate on Reynolds number.

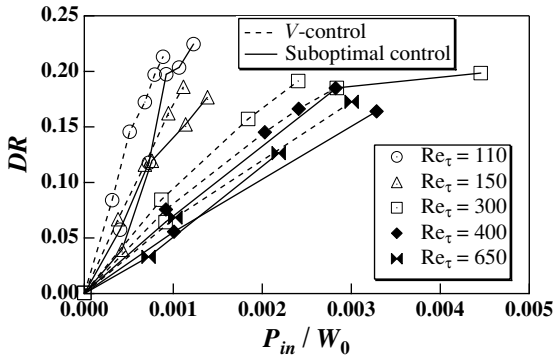

Figure 2: Drag reduction rate versus power input ratio.

input is $0.05 \sim 0.4\%$ of the pumping power. The power input P_{in} and the pumping power W are respectively defined as

$$P_{in} \equiv \overline{p_{wall} v_{wall}} + 1/2 \cdot \rho \overline{v_{wall}^3}, \tag{3}$$

and

$$W \equiv -d\bar{P}\Big/dx \cdot U_{mean}. \tag{4}$$

A fully developed flow field is used as the initial condition.

3 Reynolds Number Effect on Feedback Control

Figure 1 shows the drag reduction rate versus Re_τ for the two control schemes examined. Since the flow rate is kept constant, the drag reduction rate DR is given by

$$DR \equiv (W_0 - W)/W_0, \tag{5}$$

where W_0 denotes the pumping power for the unmanipulated flow.

The present result at $Re_\tau = 110$ is in good agreement with the DNS data of Choi et al.[7] and Lee et al.[9]; the drag reduction of about 20% is achieved with $\alpha = 1$. For the V-control scheme with constant α, DR is decreased with increasing Re_τ and eventually seems

to reach some asymptotic values. On the other hand, for the suboptimal control scheme, DR shows temporary increase and then decreases with increasing Re_τ. It is about 12% at Re_τ = 650 with $\alpha = 1$. This is probably because the suboptimal control algorithm is based on the linearized Navier-Stokes equation, although nonlinear interaction near the wall becomes more active with increasing Re_τ as described later. Recently, Collis et al.[12] made large eddy simulation of turbulent channel flow to assess the Reynolds number effect of V-control scheme and reported decrease in the control effectiveness with increasing the Reynolds number.

Figure 2 shows DR versus the power input ratio P_{in}/W_0, which corresponds to the fraction of the blowing/suction work against the pumping power. Unlike in Fig. 1, DR of the V-control scheme is decreased drastically as Re_τ is increased when P_{in}/W_0 is kept constant. However, DR gradually becomes insensitive to the Reynolds number at $Re_\tau > 300$. The present result is in accordance with the findings of Moser et al.[3] that obvious low-Reynolds-number effects are absent at $Re_\tau > 300$. Note that the V-control scheme gives slightly larger DR than the suboptimal control scheme with the same P_{in}/W_0.

In the following chapter, we analyze the DNS database using the Karhunen-Loève decomposition [13] in order to study the underlying flow mechanisms, which result in the marked Reynolds number dependence presently explored. In particular, we focus on the dynamics of coherent structures near the wall such as quasi-streamwise vortices and longitudinal streaks [14]. We also try to obtain a clue for keeping control schemes effective at higher Reynolds number flows.

4 Nonlinear Interactions between Coherent Structures

4.1 Karhunen-Loève decomposition

The Karhunen-Loève theory is based on the decomposition of the fluctuating velocity field into a sum of eigenfunctions ψ_i of the two-point correlation tensor κ_{ij} [13] as:

$$\int_0^{2\delta} \kappa_{ij}\left(y, y', m, n\right) \psi_j\left(y', m, n\right) dy' = \lambda\left(m, n\right) \psi_i\left(y, m, n\right), i, j = 1 - 3, \tag{6}$$

where m and n respectively denote wavenumbers in the x- and z-directions, while λ denotes the eigenvalue. The total number of eigenvalues for wavenumber index pairs (m, n) is three times of N_y, which is the number of grid points in the y-direction. Each eigenfunction is specified with a triplet $k = (m, n, q)$ [15].

4.2 Turbulent kinetic energy of KL modes

Figure 3 shows the normalized cumulative energy summation of the KL modes at each Reynolds number. It is found that the convergence becomes slower with increasing the Reynolds number, although only 190, 340, and 760 eigenfunctions can represent 50% of the total kinetic energy at Re_τ = 110, 300, and 650, respectively.

Figure 4 shows the most energetic eigenfunctions among the KL modes. For all Reynolds numbers, δ-scale low- and high-speed regions associated with streamwise vortices are observed. They are homogeneous ($m = 0$) in the streamwise direction at Re_τ = 110 and 300, but not (m = 1) at Re_τ = 650. Although it is not shown here, KL modes containing streamwise vortices near the wall have the largest contribution to the wall shear stress fluctuations at all Reynolds numbers.

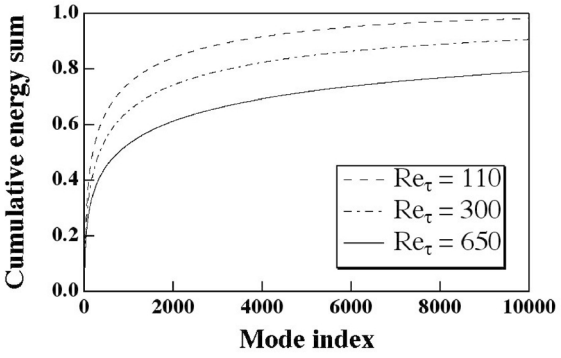

Figure 3: Cumulative energy summation of the KL modes.

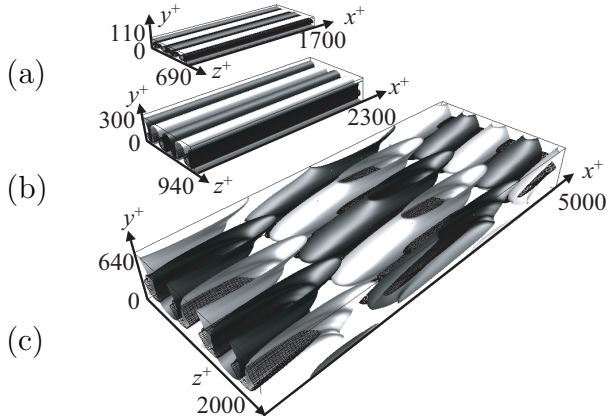

Figure 4: Most energetic eigenfunction among the KL modes. Isosurfaces of u'^+ and the second invariant of the deformation tensor Q^+ are shown. White, $u'^+ = 0.15$; black, u'^+ = -015; mesh, $Q^+ = 0$. (a)$Re_\tau = 110$, (b)$Re_\tau = 300$, (c)$Re_\tau = 650$.

In order to investigate the dynamics of coherent structures in detail, wall elevation of these structure is characterized with the center of the vortices y_v for each KL mode defined by the global minimum of the second invariant of the deformation tensor Q^+ [10]. Then, the KL modes are divided into subgroups depending on the location of the center of the vortices y_v. The n-th subgroup $u_i^{<n>}$ is composed of linear superposition of the KL modes, of which y_v exist in between y_{n-1} and y_n:

$$u_i^{<n>}(x,y,z,t) = \sum_{y_{n-1}<y_v<y_n} a^k(t)\,\phi_i^k(x,y,z), \tag{7}$$

where ϕ_i is the eigenfunction in physical space, $y_i^+ = 5 \cdot 1.5^{i-1}, i \geq 1$ and $y_0^+ = 0$ for all Reynolds numbers. Hence, the number of subgroups are 9, 11, and 13 for $Re_\tau = 110$, 300, and 650, respectively. Because of the linear superposition of the KL modes, each subgroup as a whole also satisfies the incompressibility, the no-slip boundary condition and the orthogonality. Hereafter, quantities of the subgroup $u^{<n>}$ is plotted at $y_s = 0.5(y_{n-1} + y_n)$ in all figures.

Figure 5 shows an instantaneous flow field for $Re_\tau = 110$, in which both the near-wall vortical structures and those of the subgroup of $y_s^+ = 21$ are represented. Both of them are visualized with the 3-D contours of the second invariant of the deformation tensor $Q^+(= u_{i,j}^+ u_{j,i}^+) = -0.02$. It is found that the trace of the subgroup almost always correspond to the leg vortices in the instantaneous flow field, and the wall elevation of these structures is around $y^+ = 21$, that is $y^+ = y_s^+$. Thus, the subgroup mainly represents the instantaneous vortical structures around $y^+ = y_s^+$. It is noted that subgroups of different y_s^+ also represents the instantaneous vortices around $y^+ = y_s^+$(not show here).

4.3 Contribution of KL subgroups to Reynolds shear stress

The Reynolds shear stress can be written using the KL subgroups as

$$\overline{-u'v'} = \sum_n \overline{-u^{<n>}v^{<n>}} + \sum_m \sum_{n(\neq m)} \overline{-u^{<m>}v^{<n>}}, \tag{8}$$

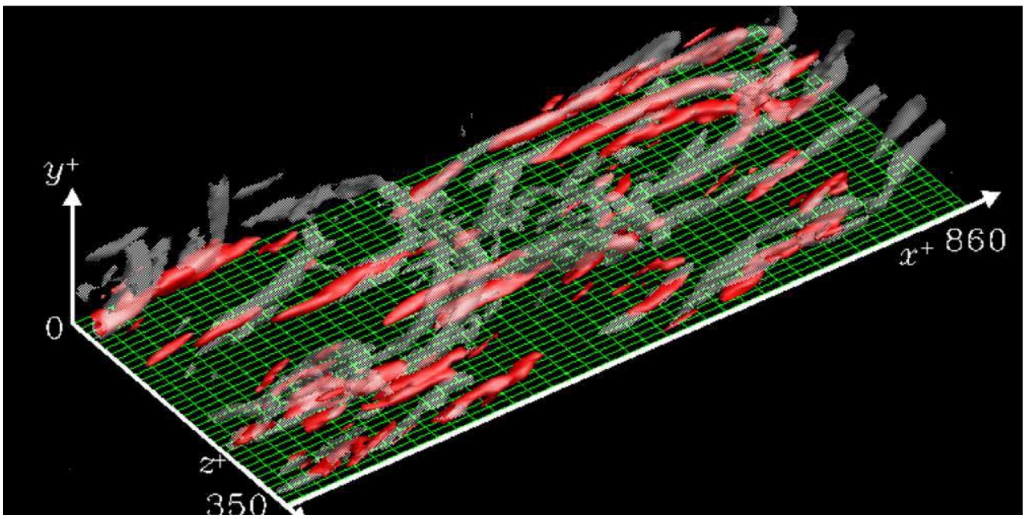

Figure 5: Near-wall coherent structures for $Re_\tau = 110$ (translucent gray, the second invariant of the deformation tensor ($Q^+ < -0.02$); red, the second invariant of the deformation tensor of the subgroup of $y_s^+ = 21$ ($Q^+ < -0.02$)).

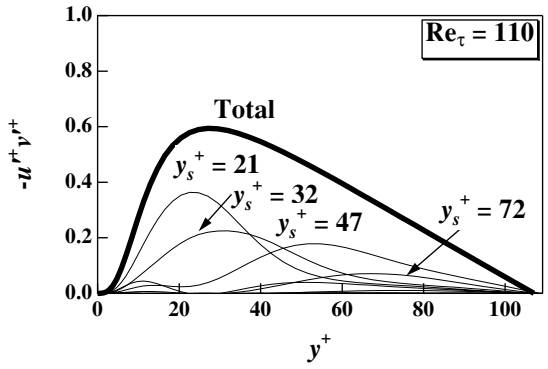

Figure 6: Contribution of KL subgroup to the Reynolds shear stress at $Re_\tau = 110$

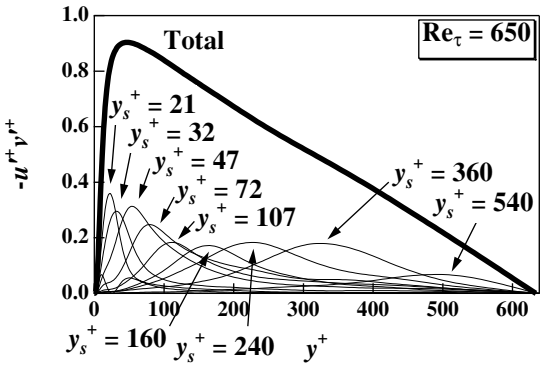

Figure 7: Contribution of KL subgroup to the Reynolds shear stress at $Re_\tau = 650$

where the first term of RHS corresponds to the correlation between the same KL subgroup, while the second term is that between different subgroups. It is found that the latter is less than 1% of the former and is negligible.

Figure 6 shows the contribution of typical KL subgroups to the Reynolds shear stress for $Re_\tau = 110$. The peak location of each subgroup is $y^+ \approx y_s^+$, which means that the KL subgroups mainly contribute to the Reynolds stress near the vortex center. The subgroup of $y_s^+ = 21$ dominates close to the wall ($y^+ < 20$), and the contribution of the subgroups of $y_s^+ > 47$ is small. On the other hand, when $Re_\tau = 650$ (Figure 7), not only the near-wall subgroups but also the subgroups away from the wall ($y_s^+ \leq 360$) have large contribution to the Reynolds stress.

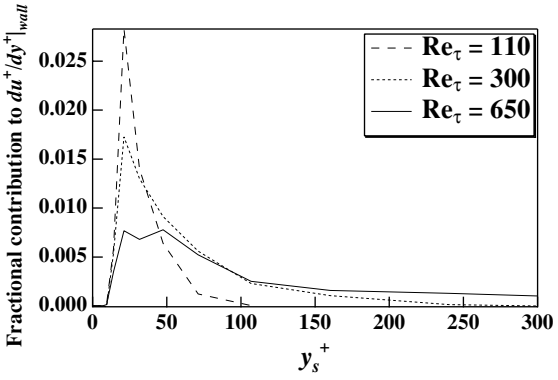

Figure 8: Fractional contribution of each KL subgroup to the wall friction increase beyond the laminar value.

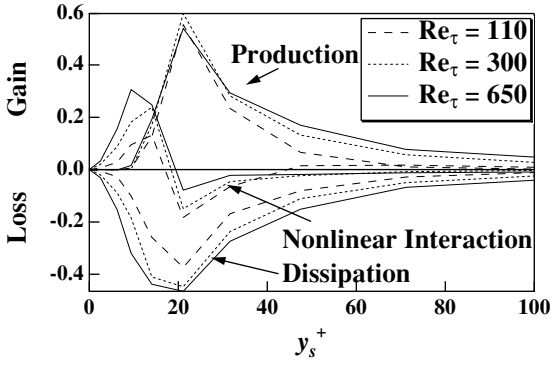

Figure 9: Energy budget of KL subgroup

4.4 Contribution of KL subgroups to mean wall shear stress

The total shear stress τ in the turbulent channel flow is given as

$$\tau = \mu \left.\frac{\partial \overline{u}}{\partial y}\right|_{wall} \left(1 - \frac{y}{\delta}\right) = \mu \frac{\partial \overline{u}}{\partial y} - \rho \overline{u'v'}. \tag{9}$$

Then, by integrating Eq. (9) twice in the y-direction [16], the mean wall shear stress can be written with the bulk mean velocity and the Reynolds shear stress as;

$$\left.\frac{\partial \overline{u^+}}{\partial y^+}\right|_{wall} = \frac{3}{Re_\tau} \overline{u^+}_{mean} + \frac{3}{Re_\tau} \int_0^{\delta^+} \overline{-u'^+ v'^+} \left(1 - \frac{y^+}{Re_\tau}\right) dy^+. \tag{10}$$

The first term of RHS represents the wall shear stress for the laminar flow with same flow rate. Under the constant flow-rate condition, the first term of RHS is also constant at each Reynolds number and is about 0.38, 0.17, and 0.09 for $Re_\tau = 110$, 300, and 650, respectively. The second term represents the contribution of the Reynolds shear stress to the wall shear stress. Thus, the second term of RHS must be decreased in order to reduce the wall shear stress in turbulent flows.

Figure 8 shows the fractional contribution of each KL subgroup to the second term of RHS in Eq. (10). For $Re_\tau = 110$, the contribution of the subgroups around $y_s^+ = 21$ is dominant, indicating that large drag reduction could be achieved only if the near-wall subgroups are suppressed. When the Reynolds number increases, the contribution of the near- wall subgroups is drastically decreased, while those of the subgroups of $y_s^+ > 50$ are increased. Therefore, for the higher Reynolds number, the subgroups away from the wall should also be suppressed in order to obtain the same degree of drag reduction.

4.5 Nonlinear interactions between KL subgroups

The energy balance equation of $u_i^{<n>}$ is derived as

$$0 = \sum_m \overline{-u_i^{+<n>} \cdot u_j^{+<m>} \cdot U_{i,j}^+} - \sum_m \overline{u_{i,j}^{+<n>} \cdot u_{i,j}^{+<m>}} + \sum_{m(\neq n)} \overline{-u_i^{+<n>} \cdot u_j^+ \cdot u_{i,j}^{+<m>}}, \tag{11}$$

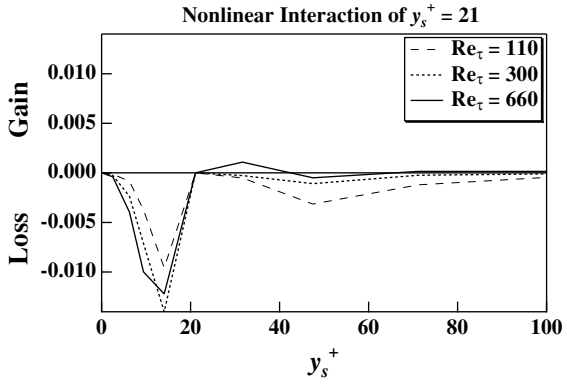

Figure 10: Nonlinear interaction term of the subgroup of $y_s^+ = 21$.

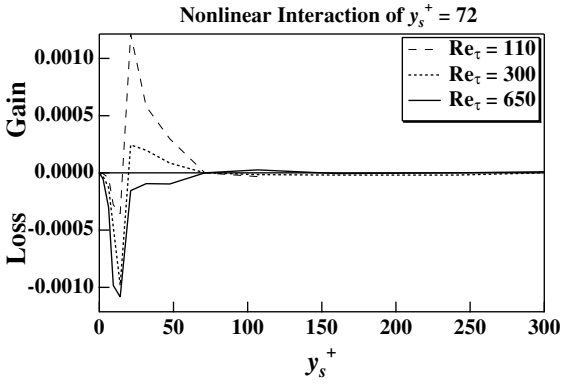

Figure 11: Nonlinear interaction term of the subgroup of $y_s^+ = 72$.

where the three terms of RHS respectively correspond to the production, dissipation and nonlinear interaction between subgroups (NL). The over bar in Eq. (11) denotes the time-space average.

Figure 9 shows the three terms of Eq. (11) of each KL subgroup for all Reynolds numbers. For $Re_\tau = 110$, the subgroups below $y_s^+ = 10$ have no production, and only dissipate the energy transferred from other subgroups through NL. The subgroup of $y_s^+ = 21$, which corresponds to the streamwise vortices, has the largest production. About one third of the energy produced is transferred to the other subgroups through NL, whereas the rest is dissipated. All the terms become smaller with increasing y_s, but the absolute value of NL is larger than 10% of that of the production term at each subgroup. Therefore, NL plays an important role in the energy budget. Note that NL is only negative at $17 < y_s^+ < 45$, which shows similar trend with the turbulent diffusion of the total turbulent kinetic energy. It is also noted that the production and dissipation terms (the first two terms of Eq. (11)) have a finite value only when $m = n$ (not shown).

When the Reynolds number increases, the subgroups below $y_s^+ = 10$ gain larger energy from the other subgroups through NL. Production of the subgroups of $y_s^+ = 21$ remains unchanged, while NL energy transfer to the other subgroups is decreased. For $y_s^+ > 45$, NL becomes negative, which implies that the vortices away from the wall transfer their energy to the other subgroups through NL.

Figure 10 shows the nonlinear interaction term of the subgroup of $y_s^+ = 21$, which corresponds to the near-wall streamwise vortices. For $Re_\tau = 110$, the energy is transferred not only to the near-wall subgroups but also to the subgroups away from the wall. When the Reynolds number increases, the energy is only transferred to the near wall subgroups. Therefore, the net nonlinear interaction term only acts as inward energy transfer.

Figure 11 shows the nonlinear interaction term of the subgroup of $y_s^+ = 72$. For $Re_\tau = 110$, the subgroup gains the energy from the subgroups of $14 < y_s^+ < 72$, and loses the energy to the subgroups of $y_s^+ < 14$. For $Re_\tau = 650$, on the other hand, the subgroup only loses the energy to the subgroups of $y_s^+ < 72$. Therefore, the outward energy transfer becomes smaller, and the inward energy transfer becomes larger with increasing the Reynolds number. We also found that there is very small direct interaction between the subgroup of $y_s^+ = 72$ and outer ($y_s^+ > 100$) layers even at $Re_\tau = 650$. Note that the tendency of the subgroups of $y_s^+ < 100$ is almost same as that of $y_s^+ = 72$(not shown here).

Previous studies have shown that the near-wall structures are self-sustained through regeneration mechanisms [17, 18]. Recently, Jimenez & Pinelli [19] claim that the damping of velocity fluctuations at $y^+ < 60$ results in laminarization, whilst the near-wall turbulence remains mostly unchanged when all the velocity fluctuations at $y^+ > 60$ are filtered out. The present findings with the KL decomposition demonstrate quantitatively that the near-wall turbulence mechanism depends only on the structures near the wall, say around $y^+ < 100$, even at $Re_\tau = 650$. Therefore, more efficient feedback control algorithm can be developed by considering near-wall dynamics at $y^+ < 100$.

5 Conclusions

Direct numerical simulation of turbulent channel flow was made in order to assess the performance of feedback control algorithms. KL decomposition is applied to examine quantitatively the effect of interaction between near-wall and outer layer structures. The following conclusions are derived:

1. The V-control scheme offers substantial drag reduction rate for all Reynolds numbers examined, but the efficiency of the control is markedly deteriorated when the Reynolds number is increased. It is mainly owing to the increase of pressure fluctuation on the wall. The drag reduction rate and efficiency of the suboptimal control scheme are smaller than those of V-control scheme at the same Reynolds number and power input.

2. The KL modes around $y^+ = 20$, which corresponds to the near-wall streamwise vortices, have large contribution not only to the Reynolds stress but also to the mean wall shear stress at $Re_\tau = 110$. However, the contribution of the KL modes away from the wall becomes larger with increasing Reynolds number.

3. When $Re_\tau = 110$, most of the turbulence energy is generated in the KL subgroups around $y^+ = 20$ and redistributed toward/away from the wall. On the other hand, when the Reynolds number is increased, the nonlinear interaction among the inner layer structures ($y^+ < 100$) acts as the energy transfer toward the wall. The direct interaction between inner ($y^+ < 100$) and outer ($y^+ > 100$) layers is inactive even at $Re_\tau = 650$. Therefore, coherent structures at $y^+ < 100$ should be manipulated in efficient feedback control scheme for higher Reynolds number flows.

6 Acknowledgments

This work was supported through the Grant-in-Aid for Science Research on Priority Areas (B) by the Ministry of Education, Culture, Sports, Science and Technology of Japan (MEXT).

References

[1] Robinson, S. K., 1991. Coherent motions in the turbulent boundary layer. Annu. Rev. Fluid Mech. 23, 601-639.

[2] Kasagi, N., Sumitani, Y., Suzuki, Y., and Iida, O., 1995. Kinematics of the quasi-coherent vortical structure in near-wall turbulence. Int. J. Heat & Fluid Flow 16, 2-10.

[3] Moser, R. D., Kim, J., and Mansour, N. N., 1999. Direct numerical simulation of turbulent channel flow up to $Re_\tau = 590$. Phys. Fluids 11, 4, 943-945.

[4] Adrian, R. J., Meinhart, C. D., and Tomkins, C. D., 2000. Vortex organization in the outer region of the turbulent boundary layer. J. Fluid Mech. 422, 1-54.

[5] Moin, P., and Bewley, T., 1994. Feedback control of turbulence. Appl. Mech. Rev. 47, S3-S13.

[6] Kasagi, N., 1998. Progress in direct numerical simulation of turbulent transport and its control. Int. J. Heat & Fluid flow 19, 125-134.

[7] Choi, H., Moin, P., and Kim, J., 1994. Active turbulence control for drag reduction in wall-bounded flows. J. Fluid Mech. 262, 75-110.

[8] Bewley, T. R., Moin, P., and Temam, R., 2001. DNS-based predictive control of turbulence: an optimal benchmark for feedback algorithms. J. Fluid Mech. 447, 179-225.

[9] Lee, C., Kim, J., and Choi, H., 1998. Suboptimal control of turbulent channel flow for drag reduction. J. Fluid. Mech. 358, 245-258.

[10] Iwamoto, K., Suzuki, Y., and Kasagi, N., 2002. Reynolds number effect on wall turbulence: toward effective feedback control. Int. J. Heat & Fluid flow 23, 678-589.

[11] Kim, J., Moin, P., and Moser, R., 1987. Turbulence statistics in fully developed channel flow at low Reynolds number. J. Fluid Mech. 177, 133-166.

[12] Collis, S. S., Chang, Y., Kellogg, S., and Prabhu, R. D., 2000. Large eddy simulation and turbulence control. AIAA paper 2000-2564.

[13] Lumley, J. L., 1970. Stochastic tools in turbulence. Academic.

[14] Kline, S. J., Reynolds, W. C., Schraub, F. A., and Runstadler, P. W., 1967. The structure of turbulent boundary layers. J. Fluid Mech. 30, 741-773.

[15] Webber, G. A., Handler, R. A., and Sirovich, L., 1997. The Karhunen-Loève decomposition of minimal channel flow. Phys. Fluids 9, 1054-1066.

[16] Fukagata, K., Iwamoto, K., and Kasagi, N., 2002. Contribution of Reynolds stress distribution to the skin friction in wall-bounded flows. Phys. Fluids, to appear.

[17] Hamilton, J. M., Kim, J., and Waleffe F., 1995. Regeneration mechanisms of near-wall turbulence structures. J. Fluid Mech. 287, 317-348.

[18] Jeong, J., Hussain, F., Schoppa, W., and Kim, J., 1997. Coherent structures near the wall in a turbulent channel flow. J. Fluid Mech. 332, 185-214.

[19] Jimenez, J., and Pinelli, A., 1999. The autonomous cycle of near-wall turbulence. J. Fluid Mech. 389, 335-359.